Title
First-Principles Analysis of Radiative Recombination in Lead-Halide Perovskites

Journal
ACS Energy Letters, 3(10)

ISSN
2380-8195

Authors
Zhang, Xie
Shen, Jimmy-Xuan
Wang, Wennie
et al.

Publication Date
2018-10-12

DOI
10.1021/acsenergylett.8b01297

Peer reviewed

First-Principles Analysis of Radiative Recombination in Lead-Halide Perovskites

Xie Zhang,*,†,¶ Jimmy-Xuan Shen,‡,¶ Wennie Wang,† and Chris G. Van de Walle*,†

†*Materials Department, University of California, Santa Barbara, CA 93106-5050, United States*

‡*Department of Physics, University of California, Santa Barbara, CA 93106-9530, United States*

¶*Contributed equally to this work*

E-mail: xiezhang@ucsb.edu; vandewalle@mrl.ucsb.edu

Abstract

Slow radiative recombination due to a slightly indirect band gap has been proposed to explain the high efficiency of lead-halide perovskite solar cells. Here, we calculate the radiative recombination rate from first principles for the prototypical lead-halide perovskite, $MAPbI_3$ ($MA=CH_3NH_3$). Since the structure is dynamic, with the MA molecule rotating even at room temperature, we determine the momentum mismatch between the band edges as a function of the orientation of the MA molecule. Our results demonstrate that the indirect nature of the band gap suppresses the radiative recombination rate by less than a factor of two, and that the radiative recombination coefficient is as high as in traditional direct-gap semiconductors. Our study provides a rigorous assessment of the radiative recombination mechanisms and their relation to the high efficiency of lead-halide perovskite solar cells, and will provide a sound basis for accurate modeling.

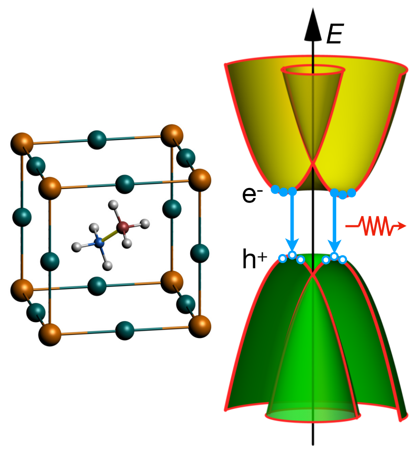

Lead-halide perovskites are strong candidates for next-generation solar cells, since they can be cheaply fabricated and exhibit photovoltaic efficiencies greater than 22%.[1] Extensive studies have been aimed at understanding the high efficiency of these materials. The radiative recombination rate has attracted a lot of attention; it was suggested that the radiative recombination coefficient should be low in order to avoid undesired carrier recombination.[2–11] A significant reduction of the radiative recombination rate was attributed to the formation of an indirect band gap due to strong spin-orbit coupling (SOC).

In this work, we perform a comprehensive first-principles study of radiative recombination rates and the mechanisms by which they are governed. We compute the radiative recombination coefficient (B) in the prototypical lead-halide perovskite, $MAPbI_3$ ($MA{=}CH_3NH_3$), and analyze the results as a function of carrier density. The value of the recombination coefficient depends on the details of the atomic structure; this structure is dynamic, even at room temperature, because the MA molecule can easily rotate. The orientation of the molecule leads to a polar distortion, which causes SOC-induced momentum splittings at the conduction-band minimum (CBM) and valence-band maximum (VBM). This momentum mismatch, in turn, affects radiative recombination. However, we find that the mismatch changes the room-temperature B coefficient by less than a factor of two, with values ranging from 0.6×10^{-10} to 1.1×10^{-10} cm^{3}s^{-1} at typical solar-cell carrier densities. These values are comparable to those in traditional III-V semiconductors with direct band gaps. Our first-principles analysis thus shows that the indirect nature of the band gap has only a minor impact on radiative recombination.

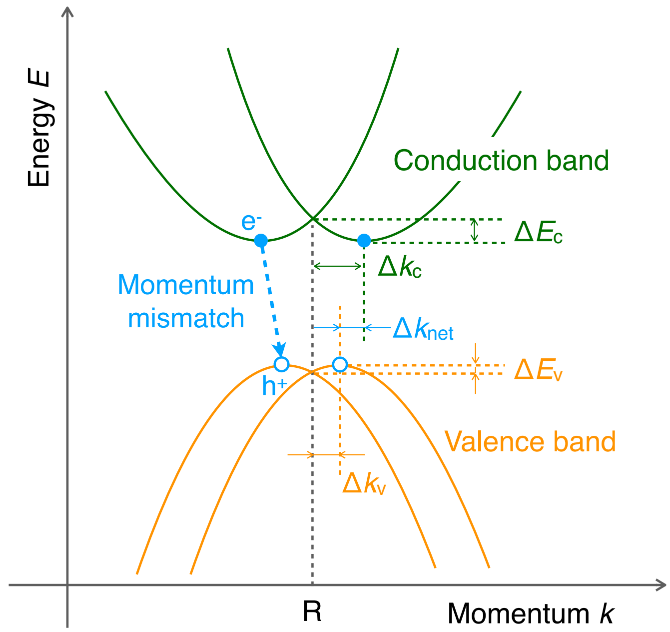

Figure 1: Schematic of energy-versus-momentum diagram near the band extrema in $MAPbI_3$, illustrating momentum mismatch. The light-blue solid circles denote photogenerated electrons (e^-); light-blue open circles holes (h^+).

Figure 1 shows how an indirect band gap can suppress radiative recombination. At typical carrier densities in solar cells the photogenerated electrons and holes are highly concentrated in a small region near the band extrema. Since radiative recombination must conserve momentum, it is significantly reduced if there is a momentum mismatch between the CBM and VBM.

The suppression of radiative recombination depends sensitively on the details of the band structure. The splittings of the bands at the CBM and VBM can be characterized by the quantities Δk_c, Δk_v, Δk_{net}, ΔE_c and ΔE_v, as shown in Figure 1. We find that the CBM and VBM are both comprised of a ring of states in the three-dimensional Brillouin zone, and we define the splittings Δk_c and Δk_v as the ones where ΔE_c and ΔE_v have the largest magnitude among all directions in **k** space. The **k**-space shifts are in principle vector quantities, but we verified that in all cases $\Delta \mathbf{k}_c$ and $\Delta \mathbf{k}_v$ are close to collinear. Δk_c, Δk_v and Δk_{net} thus

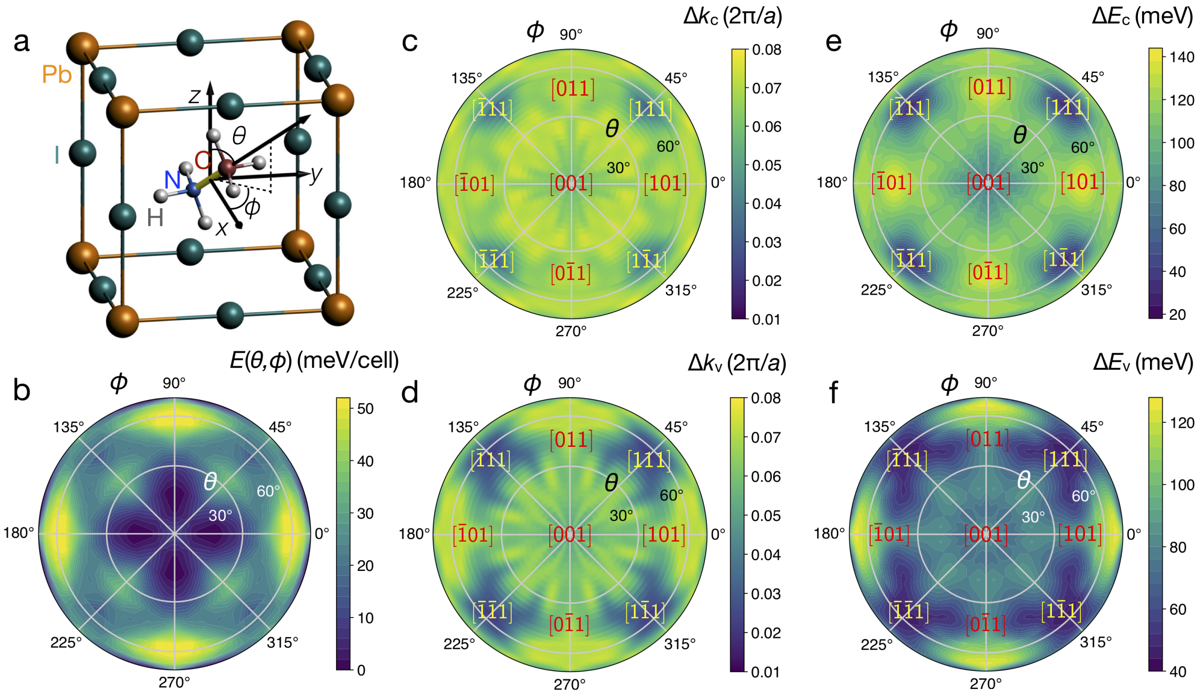

Figure 2: (a) Crystal structure of $MAPbI_3$. The MA orientation is characterized by the angles θ and ϕ. (b) Energy $E(\theta,\phi)$ of a $MAPbI_3$ unit cell as a function of θ and ϕ, referenced to the energy minimum as a function of MA orientation. (c, d) Momentum splitting at the CBM (Δk_{c}) and VBM (Δk_{v}) as a function of θ and ϕ. (e, f) Energy splitting at the CBM (ΔE_{c}) and VBM (ΔE_{v}) as a function of θ and ϕ.

provide information about the **k**-space separation of the electrons and holes. ΔE_{c} and ΔE_{v} relate to the curvature at the band edges and the density of states, and thus to the *range* of momenta of the states occupied by electrons and holes.

A reliable assessment of the impact of momentum mismatch requires the accurate computation of the band structure and wavefunctions. Here we use density functional theory with a hybrid functional, which has been demonstrated to provide reliable atomic and electronic structures.[12] We have shown[13] that phenomenological models (such as a Rashba Hamiltonian within a tight-binding model[2]) can lead to an incorrect description of spin orientations at the band edges. Such inaccuracies can lead to a significant suppression of radiative recombination rates. Still, it is unclear how strong the impact of momentum mismatch on the radiative recombination rates is, which will be quantitatively addressed in the present study.

An additional challenge is that the band structure is not static but dynamic, since the

MA molecule is rotating at room temperature. The band-structure splitting is a result of SOC acting on an atomic structure that lacks inversion symmetry, and it has been noted (e.g., in Ref. 3) that the splitting depends on the orientation of the MA molecule. The dynamics of the MA rotation has already been addressed by Mattoni *et al.*[14] and Lahnsteiner *et al.*[15] with molecular dynamics simulations. The evolution of the MA orientation and the momentum splitting with time was revealed. However, a systematic assessment of the details of the splittings as a function of the MA orientation, and their quantitative impact on the B coefficient, is still missing. In the present study we vary the MA orientation and explicitly compute the corresponding band-structure splittings from first principles. Since we want to sample a large number of MA orientations, use of a hybrid functional would be computationally prohibitive; we therefore use the functional of Perdew, Becke, and Ernzerhof (PBE).[16] Our benchmark comparisons with the hybrid functional of Heyd, Scuseria, and Ernzerhof (HSE)[17] show that PBE produces the same trends as HSE, but tends to overestimate distortions of Pb-I octahedra, and thus Δk and ΔE. For the purposes of the present study, this strengthens our conclusion that the momentum mismatch does not have a major impact on radiative recombination.

Figure 2a defines the angles θ ([0, 90°]) and ϕ ([0, 360°]) that characterize the orientation of the MA molecule in the cubic unit cell of $MAPbI_3$. Figure 2b presents the energy of $MAPbI_3$ as a function of the MA orientation. The energy varies over a range of less than 55 meV per (12-atom) unit cell, implying that even at room temperature the material adopts different structures corresponding to different MA orientations, as has indeed been experimentally observed (e.g., Ref. 18). Figure 2c,d shows the corresponding momentum splittings. Except for a small region around the $\langle 111 \rangle$ orientation, both Δk_c and Δk_v are large, on the order of 0.07 (in units of $2\pi/a$, where a is the lattice constant). Importantly, however, Δk_c and Δk_v are strongly correlated, and therefore Δk_{net} is small. This indicates that electrons and holes will not be far apart in momentum space. Figure 2e,f shows that the energy splittings at the CBM and VBM vary substantially with MA orientation. But similar to what we observed for the momentum splittings, ΔE_c and ΔE_v are correlated, and the extrema of $\Delta E_\mathrm{c/v}$ also occur for MA orientations around $\langle 111\rangle$ and $\langle 011\rangle$.

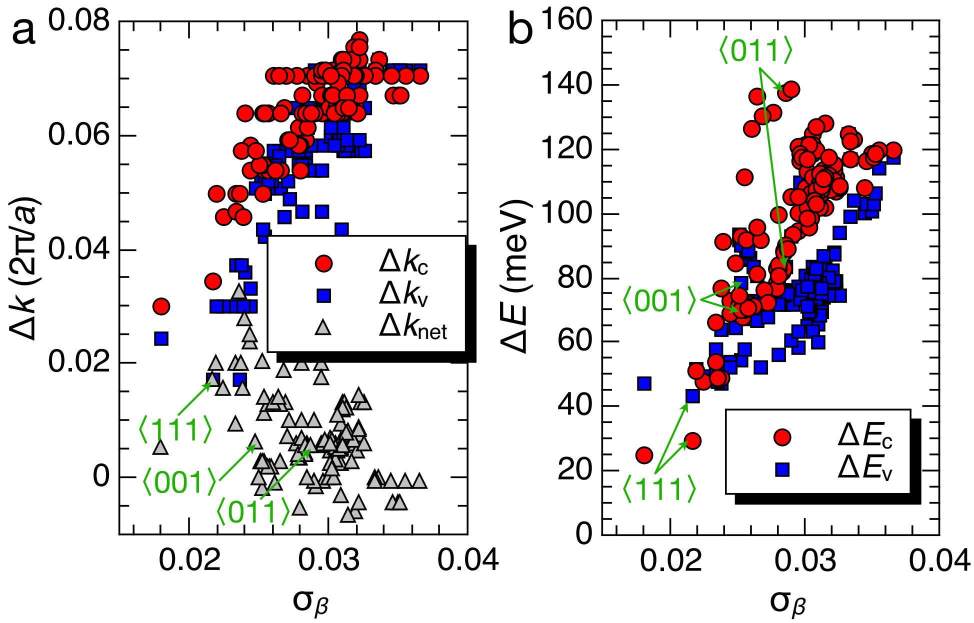

Figure 3: (a) Momentum (Δk) and (b) energy (ΔE) splittings as a function of the standard deviation in bond angles σ_β, for all sampled configurations with different MA orientations.

The strong correlation between the splittings at the CBM and VBM arises because they both originate from the inversion asymmetry of the atomic structure. The main difference between the CBM and VBM is that the CBM has Pb-p character, while the VBM has primarily I-p character, which leads to the quantitative differences in splittings. A good measure of the distortion of the perovskite structure is given by the standard deviation of the I-Pb-I bond angles:

$$\sigma_\beta = \sqrt{\sum_{i=1}^{12}(\beta_i - \pi/2)^2/11}\,, \tag{1}$$

where β_i are the 12 I-Pb-I bond angles within an octahedron.[19] In Figure 3, we plot all the momentum and energy splittings at the CBM and VBM as a function of σ_β. There are three key insights we can gain from these results. First, a larger σ_β induces larger splittings of momentum and energy for both the CBM and VBM. Second, while Δk_c and Δk_v can be large for some MA orientations, they are strongly correlated and therefore Δk_net is overall small for all MA orientations, and actually decreases with increasing distortion [Figure 3a]. Since our detailed tests show that PBE tends to overestimate the distortions, the splittings as obtained from HSE calculations will be even smaller. Thus, the impact of Δk_{net} on the radiative recombination coefficient is expected to be minor. Third, the $\Delta E_{\mathrm{c/v}}$ values vary significantly between different MA orientations [Figure 3b], which may affect the occupation of carriers in the vicinity of the CBM and VBM, and could impact the B coefficient.

The evaluations of Δk and ΔE for various configurations provide valuable insights, but ultimately the impact on radiative recombination needs to be assessed by explicit calculations that take the occupation of states by electrons and holes into account. To achieve this, we perform first-principles computations for the B coefficient, using hybrid-functional calculations for atomic and electronic structure and momentum matrix elements (see the Methods section for details). It would be too computationally demanding to do this for all of the MA orientations, but as discussed above the spread of the B coefficient due to varied MA orientations is determined by the $\Delta E_{\mathrm{c/v}}$ value. As marked in Figure 3b the extrema of $\Delta E_{\mathrm{c/v}}$ occur around $\langle 011 \rangle$ and $\langle 111 \rangle$ orientations, with $\langle 001 \rangle$ giving intermediate values. Focusing on these high-symmetry orientations thus allows us to capture the range of B coefficients.

As a check of the reliability of the PBE results reported in Figures 2 and 3, we calculated the B coefficient (using HSE for computing eigenvalues and momentum matrix elements) for the PBE-relaxed configuration of the [011] MA orientation. We found that the B coefficients for the HSE and PBE structures agree to within 20%, providing confidence in the reliability of the PBE results.

Figure 4 shows the calculated B coefficients for all three orientations. It is clear that the MA orientation does not have a major impact on radiative recombination rates. The $\langle 111 \rangle$ orientation corresponds to a "best case" scenario, since it has almost the lowest ΔE, while $\langle 011 \rangle$ is close to a "worst case"; still, changing the orientation from $\langle 111 \rangle$ to $\langle 011 \rangle$ decreases the B coefficient by less than a factor of two instead of more than two orders of magnitude in the literature.[4] In the present study, all MA molecules are aligned to the same orientation

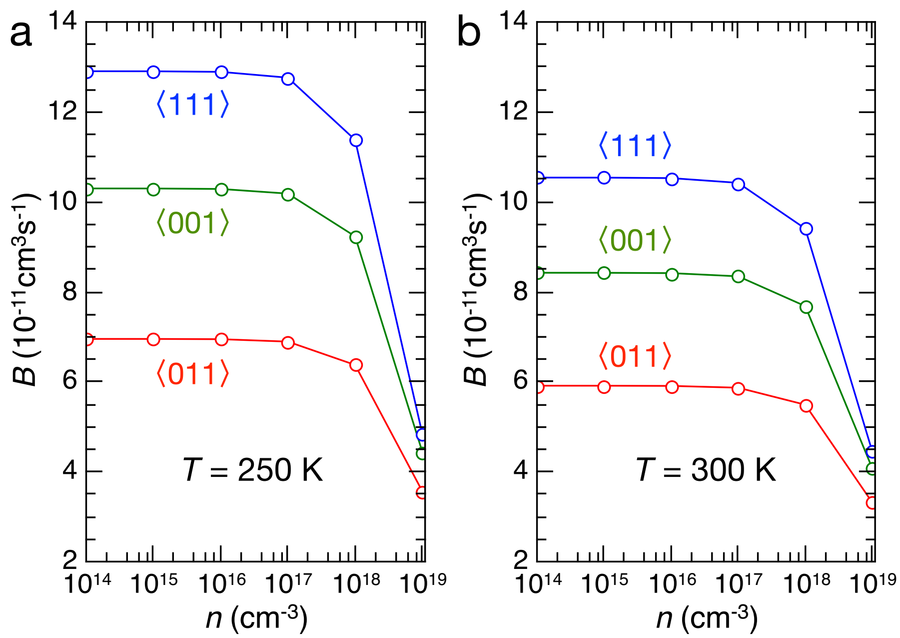

Figure 4: (a) Radiative recombination coefficients in $MAPbI_3$ with the MA molecule oriented along $\langle 111 \rangle$, $\langle 001 \rangle$, and $\langle 011 \rangle$ directions at 250 K. (b) Same quantities at 300 K.

due to the periodically repeated unit cell. In reality, the local polarization induced by a MA molecule is reduced due to nearby MA molecules with different orientations. This means that the SOC-induced splitting is even smaller in actual $MAPbI_3$. We conclude that the indirect nature of the band gap does not significantly affect radiative recombination.

Figure 4 also provides information about the temperature and carrier density dependence of B. For all three orientations the B coefficients exhibit the typical behavior familiar from other direct-gap semiconductors. As a function of temperature, B decreases with increasing temperature. As a function of carrier density, the B coefficients are almost constant up to 10^{17} cm^{-3}. Above 10^{18} cm^{-3}, the B coefficients decrease rapidly due to the well-established phase-space filling effect.[20] Since typical photogenerated carrier densities in solar cells are lower than 10^{18} cm^{-3}, the B coefficients at room temperature are in the range of $0.6 - 1.1 \times 10^{-10}$ cm^{3}s^{-1}.

Table 1 shows a comparison of our calculated B coefficient with theoretical as well as experimental values reported in the literature. With the exception of Ref. 4, the theoretical B coefficients are around $10^{-10} - 10^{-9}$ cm^{3}s^{-1}. The spread in experimental values is much

Table 1: Comparison of the calculated B coefficient in this work with various literature reports from both theory and experiment.

B coefficient (cm^3s^{-1})	Method	Source
$0.6 - 1.1 \times 10^{-10}$	First principles (HSE + SOC)	This work
$0.5 - 1.6 \times 10^{-9}$	First principles (LDA)	Filippetti *et al.*[21]
4.0×10^{-13}	First principles (GW + SOC)	Azarhoosh *et al.*[4]
1.0×10^{-9}	First principles (GW + SOC)	Davies *et al.*[22]
5.0×10^{-10}	Transient spectroscopy	Davies *et al.*[22]
6.8×10^{-10}	THz	Crothers *et al.*[23]
$0.9 - 9.4 \times 10^{-10}$	THz	Wehrenfennig *et al.*[24]
1.1×10^{-10}	THz	Wehrenfennig *et al.*[25]
2.2×10^{-8}	THz	La-o-vorakiat *et al.*[26]
6.0×10^{-11}	THz	Milot *et al.*[27]
1.7×10^{-10}	PL decay	Yamada *et al.*[28]
$2.0 - 4.0 \times 10^{-11}$	PL decay	Bi *et al.*[29]

larger; our calculated value is well within this range. The theoretical values from Filippetti *et al.*[21] and Davies *et al.*[22] are approximately one order of magnitude larger than the values reported in the present work. Filippetti *et al.* used density functional theory with the local density approximation (LDA) functional. They also did not include SOC. These limitations affect the effective masses of the band edges and hence the density of states and Fermi occupations; in addition, momentum splitting is absent. The first-principles study by Davies *et al.* focused on the orthorhombic phase, in which there is also no momentum splitting. These differences explain the higher B coefficients obtained in Refs. 21 and 22.

In summary, we have employed first-principles approaches to systematically investigate the radiative recombination in the prototypical lead-halide perovskite $MAPbI_3$. We have explicitly characterized different MA orientations and evaluated the corresponding momentum mismatch between the band edges. We find that the resulting indirect band gap leads to a variation of the radiative recombination coefficient by less than a factor of two. The computed radiative recombination coefficient is on the order of 10^{-10} cm^3s^{-1}, indicating that radiative recombination in $MAPbI_3$ is as strong as in direct-gap materials. Our results show that attempts to attribute the high efficiency of lead-halide perovskite solar cells to a suppression of radiative recombination are misguided; a low radiative recombination coefficient is not a requirement for an efficient solar cell, and attention should be focused on other recombination processes in order to explain the high solar conversion efficiency. In addition, strong radiative recombination allows a high luminescence yield, which is required for light-emitter applications.

Methods

First-principles calculations. All first-principles calculations are performed based on density functional theory and the projector augmented wave (PAW) approach[30] as implemented in the Vienna *Ab-initio* Simulation Package (VASP).[31] We use a plane-wave energy cutoff of 500 eV. The first Brillouin zone of the 12-atom unit cell of $MAPbI_3$ is sampled with a $4 \times 4 \times 4$ Monkhorst-Pack[32] **k**-point mesh. The convergence of atomic and electronic structure was checked by performing tests with a $6 \times 6 \times 6$ **k**-point mesh. The structure is relaxed for both volume and atomic positions (residual forces < 0.01 eV/Å) within the cubic shape.

We use the hybrid functional of Heyd, Scuseria, and Ernzerhof (HSE).[17] A mixing parameter $\alpha = 0.55$ yields a band gap of 1.55 eV, within the experimentally reported range of 1.5−1.6 eV,[33] and a lattice constant for the structure with [001] MA orientation of 6.348 Å, in good agreement with experiment (6.32 Å[34]).

Sampling of the MA orientation. We sample different MA orientations with a 10×40 mesh for the two angles, θ ([0, 90°]) and ϕ ([0, 360°]). All of these configurations are relaxed with constrained MA orientations. Since the lattice constant changes by less than 0.1% as a function of the MA orientation, we keep it constant (and equal to the value optimized for [001] orientation) in these calculations. To enable sampling of this large number of configurations with different MA orientations, we use the computationally less demanding generalized gradient approximation functional of Perdew, Becke, and Ernzerhof (PBE).[16] We compute the eigenvalues in the vicinity of the R point ($|k_i - \mathrm{R}_i| \leq 0.1[2\pi/a]$, where $i = x$, y and z) with a $21 \times 21 \times 21$ sampling mesh and extract the quantities Δk_c, Δk_v, Δk_{net}, ΔE_c and ΔE_v. Since the splittings depend on the inspected direction in **k** space, our computed splittings correspond to the largest ones among all directions. We have performed tests that show that even though PBE calculations underestimate the band gap, the band splittings at the CBM and VBM are qualitatively similar to the HSE values. These tests confirm that PBE calculations are reliable for capturing the overall trends.

Radiative recombination coefficients. The radiative recombination coefficient B is computed as a function of carrier density n by[35]

$$B = \frac{n_r e^2}{\pi \epsilon_0 m_e^2 c^3 \hbar^2 n^2 V} \sum_{\mathrm{cv}\mathbf{k}} f_{\mathrm{c}\mathbf{k}}(1 - f_{\mathrm{v}\mathbf{k}})(\varepsilon_{\mathrm{c}\mathbf{k}} - \varepsilon_{\mathrm{v}\mathbf{k}})|\mathbf{M}_{\mathrm{cv}\mathbf{k}}|^2, \tag{2}$$

where n_r is the refractive index of $MAPbI_3$ and is set to the experimental value[36] of 2.611. e is the elementary charge, m_e the free electron mass, ϵ_0 the vacuum permittivity, c the speed of light and V is the volume of a unit cell. $f_{\mathrm{c}\mathbf{k}}$ ($f_{\mathrm{v}\mathbf{k}}$) is the Fermi occupation factor for electrons (holes) in the CB (VB) at $\mathbf{k}$, and $\varepsilon_{\mathrm{c}\mathbf{k}}$ and $\varepsilon_{\mathrm{v}\mathbf{k}}$ are the corresponding eigenvalues. $\mathbf{M}_{\mathrm{cv}\mathbf{k}}$ is the momentum matrix element between a CB (c) and a VB (v) at $\mathbf{k}$, and an average is performed over the p_x, p_y and p_z components:

$$|\mathbf{M}_{cv\mathbf{k}}|^2 = \frac{1}{3} \sum_i |\langle \psi_{\mathrm{c}} | p_i | \psi_{\mathrm{v}} \rangle|^2, \tag{3}$$

where $i = x$, y, and z, and ψ_{c} (ψ_{v}) is the wavefunction of the CB c (VB v).

To obtain reliable B coefficients, all eigenvalues, Fermi occupations, and momentum matrix elements are based on HSE calculations including SOC. Since HSE+SOC calculations are computationally expensive, the B coefficient is computed on an adaptive $\mathbf{k}$-point mesh: in the vicinity of the R point ($|k_i - \mathrm{R}_i| \leq 0.1[2\pi/a]$, where $i =x$, y and z), a dense mesh of $21\times21\times21$ (equivalent to $100\times100\times100$ for the entire Brillouin zone) is used. The rest of the Brillouin zone is sampled on a $20 \times 20 \times 20$ mesh. For densities up to 10^{18} cm^{-3}, all occupied states lie within the denser mesh. The B coefficient is calculated by summing over all $\mathbf{k}$-points with the appropriate adaptive weight for each $\mathbf{k}$-point. In the present study we treat the electrons and holes as free carriers; Coulomb interactions between electrons and holes are not considered. As shown by Davies *et al.*,[22] this effect may increase the B coefficient by about an order of magnitude at low temperatures and by a factor of four at room temperature. Since in the present work we focus on the variation of the momentum mismatch with the MA orientation, the impact of exciton formation on the trends we identified is expected to be small.

Acknowledgement

We thank D. H. Fabini and Prof. R. Seshadri for fruitful discussions. This work was supported by the U.S. Department of Energy (DOE), Office of Science, Basic Energy Sciences (BES) under Award No. DE-SC0010689. Computational resources were provided by the National Energy Research Scientific Computing Center, a DOE Office of Science User Facility supported by the Office of Science of the U.S. Department of Energy under Contract No. DE-AC02-05CH11231.

References

(1) Yang, W. S.; Park, B.-W.; Jung, E. H.; Jeon, N. J.; Kim, Y. C.; Lee, D. U.; Shin, S. S.; Seo, J.; Kim, E. K.; Noh, J. H.; et al., Iodide Management in Formamidinium-Lead-Halide-Based Perovskite Layers for Efficient Solar Cells. *Science* **2017**, *356*, 1376–1379.

(2) Zheng, F.; Tan, L. Z.; Liu, S.; Rappe, A. M. Rashba Spin-Orbit Coupling Enhanced Carrier Lifetime in $CH_3NH_3PbI_3$. *Nano Lett.* **2015**, *15*, 7794–7800.

(3) Motta, C.; El-Mellouhi, F.; Kais, S.; Tabet, N.; Alharbi, F.; Sanvito, S. Revealing the Role of Organic Cations in Hybrid Halide Perovskite $CH_3NH_3PbI_3$. *Nat. Commun.* **2015**, *6*, 7026.

(4) Azarhoosh, P.; McKechnie, S.; Frost, J. M.; Walsh, A.; Van Schilfgaarde, M. Research

Update: Relativistic Origin of Slow Electron-Hole Recombination in Hybrid Halide Perovskite Solar Cells. *APL Mater.* **2016**, *4*, 1–8.

(5) Hutter, E. M.; Gélvez-Rueda, M. C.; Osherov, A.; Bulović, V.; Grozema, F. C.; Stranks, S. D.; Savenije, T. J. Direct-Indirect Character of the Bandgap in Methylammonium Lead Iodide Perovskite. *Nat. Mater.* **2016**, *16*, 115–120.

(6) Li, J.; Haney, P. M. Optical Spintronics in Organic-Inorganic Perovskite Photovoltaics. *Phys. Rev. B* **2016**, *93*, 1–9.

(7) Li, J.; Haney, P. M. Circular Photogalvanic Effect in Organometal Halide Perovskite $CH_3NH_3PbI_3$. *Appl. Phys. Lett.* **2016**, *109*, 193903.

(8) Moser, J.-E. Perovskite Photovoltaics: Slow Recombination Unveiled. *Nat. Mater.* **2016**, *16*, 4–6.

(9) Etienne, T.; Mosconi, E.; De Angelis, F. Dynamical Origin of the Rashba Effect in Organohalide Lead Perovskites: A Key to Suppressed Carrier Recombination in Perovskite Solar Cells? *J. Phys. Chem. Lett.* **2016**, *7*, 1638–1645.

(10) Yu, Z. G. The Rashba Effect and Indirect Electron-Hole Recombination in Hybrid Organic-Inorganic Perovskites. *Phys. Chem. Chem. Phys* **2017**, *19*, 14907.

(11) Kirchartz, T.; Rau, U. Decreasing Radiative Recombination Coefficients via an Indirect Band Gap in Lead Halide Perovskites. *J. Phys. Chem. Lett.* **2017**, *8*, 1265–1271.

(12) Franchini, C. Hybrid Functionals Applied to Perovskites. *J. Phys.: Condens. Matter* **2014**, *26*, 253202.

(13) Zhang, X.; Shen, J.-X.; Van de Walle, C. G. Three-Dimensional Spin Texture in Hybrid Perovskites and Its Impact on Optical Transitions. *J. Phys. Chem. Lett.* **2018**, *9*, 2903–2908.

(14) Mattoni, A.; Filippetti, A.; Saba, M. I.; Delugas, P. Methylammonium Rotational Dynamics in Lead Halide Perovskite by Classical Molecular Dynamics: The Role of Temperature. *J. Phys. Chem. C* **2015**, *119*, 17421–17428.

(15) Lahnsteiner, J.; Kresse, G.; Kumar, A.; Sarma, D. D.; Franchini, C.; Bokdam, M. Room-Temperature Dynamic Correlation Between Methylammonium Molecules in Lead-Iodine Based Perovskites: An Ab Initio Molecular Dynamics Perspective. *Phys. Rev. B* **2016**, *94*, 214114.

(16) Perdew, J. P.; Burke, K.; Ernzerhof, M. Generalized Gradient Approximation Made Simple. *Phys. Rev. Lett.* **1996**, *77*, 3865–3868.

(17) Heyd, J.; Scuseria, G. E.; Ernzerhof, M. Hybrid Functionals Based on a Screened Coulomb Potential. *J. Chem. Phys.* **2003**, *118*, 8207–8215.

(18) Bakulin, A. A.; Selig, O.; Bakker, H. J.; Rezus, Y. L. A.; Müller, C.; Glaser, T.; Lovrincic, R.; Sun, Z.; Chen, Z.; Walsh, A.; et al., Real-Time Observation of Organic Cation Reorientation in Methylammonium Lead Iodide Perovskites. *J. Phys. Chem. Lett.* **2015**, *6*, 3663–3669.

(19) Robinson, K.; Gibbs, G. V.; Ribbe, P. H. Quadratic Elongation: A Quantitative Measure of Distortion in Coordination Polyhedra. *Science* **1971**, *172*, 567–570.

(20) Hader, J.; Moloney, J. V.; Koch, S. W. Beyond the ABC: Carrier Recombination in Semiconductor Lasers. Proceedings of SPIE. 2006; p 61151T.

(21) Filippetti, A.; Delugas, P.; Mattoni, A. Radiative Recombination and Photoconversion of Methylammonium Lead Iodide Perovskite by First Principles: Properties of an Inorganic Semiconductor within a Hybrid Body. *J. Phys. Chem. C* **2014**, *118*, 24843–24853.

(22) Davies, C. L.; Filip, M. R.; Patel, J. B.; Crothers, T. W.; Verdi, C.; Wright, A. D.; Milot, R. L.; Giustino, F.; Johnston, M. B.; Herz, L. M. Bimolecular Recombination in Methylammonium Lead Triiodide Perovskite is an Inverse Absorption Process. *Nat. Commun.* **2018**, *9*, 293.

(23) Crothers, T. W.; Milot, R. L.; Patel, J. B.; Parrott, E. S.; Schlipf, J.; Müller-Buschbaum, P.; Johnston, M. B.; Herz, L. M. Photon Reabsorption Masks Intrinsic Bimolecular Charge-Carrier Recombination in $CH_3NH_3PbI_3$ Perovskite. *Nano Lett.* **2017**, 5782–5789.

(24) Wehrenfennig, C.; Eperon, G. E.; Johnston, M. B.; Snaith, H. J.; Herz, L. M. High Charge Carrier Mobilities and Lifetimes in Organolead Trihalide Perovskites. *Adv. Mater.* **2014**, *26*, 1584–1589.

(25) Wehrenfennig, C.; Liu, M.; Snaith, H. J.; Johnston, M. B.; Herz, L. M. Charge-Carrier Dynamics in Vapour-Deposited Films of the Organolead Halide Perovskite $CH_3NH_3PbI_{3-x}Cl_x$. *Energy Environ. Sci.* **2014**, *7*, 2269–2275.

(26) La-o vorakiat, C.; Salim, T.; Kadro, J.; Khuc, M.-T.; Haselsberger, R.; Cheng, L.; Xia, H.; Gurzadyan, G. G.; Su, H.; Lam, Y. M.; et al., Elucidating the Role of Disorder and Free-Carrier Recombination Kinetics in $CH_3NH_3PbI_3$ Perovskite Films. *Nat. Commun.* **2015**, *6*, 7903.

(27) Milot, R. L.; Eperon, G. E.; Snaith, H. J.; Johnston, M. B.; Herz, L. M. Temperature-Dependent Charge-Carrier Dynamics in $CH_3NH_3PbI_3$ Perovskite Thin Films. *Adv. Funct. Mater.* **2015**, *25*, 6218–6227.

(28) Yamada, Y.; Nakamura, T.; Endo, M.; Wakamiya, A.; Kanemitsu, Y. Photocarrier Recombination Dynamics in Perovskite $CH_3NH_3PbI_3$ for Solar Cell Applications. *J. Am. Chem. Soc.* **2014**, *136*, 11610–11613.

(29) Bi, D.; Tress, W.; Dar, M. I.; Gao, P.; Luo, J.; Renevier, C.; Schenk, K.; Abate, A.; Giordano, F.; Correa Baena, J.-P.; et al., Efficient Luminescent Solar Cells Based on Tailored Mixed-Cation Perovskites. *Sci. Adv.* **2016**, *2*, e1501170–e1501170.

(30) Blöchl, P. E. Projector Augmented-Wave Method. *Phys. Rev. B* **1994**, *50*, 17953–17979.

(31) Kresse, G.; Furthmüller, J. Efficient Iterative Schemes for Ab Initio Total-Energy Calculations Using a Plane-Wave Basis Set. *Phys. Rev. B* **1996**, *54*, 11169–11186.

(32) Monkhorst, H. J.; Pack, J. D. Special Points for Brillouin-Zone Integrations. *Phys. Rev. B* **1976**, *13*, 5188–5192.

(33) Leguy, A. M. A.; Azarhoosh, P.; Alonso, M. I.; Campoy-Quiles, M.; Weber, O. J.; Yao, J.; Bryant, D.; Weller, M. T.; Nelson, J.; Walsh, A.; et al., Experimental and Theoretical Optical Properties of Methylammonium Lead Halide Perovskites. *Nanoscale* **2016**, *8*, 6317–6327.

(34) Weller, M. T.; Weber, O. J.; Henry, P. F.; Di Pumpo, A. M.; Hansen, T. C. Complete Structure and Cation Orientation in the Perovskite Photovoltaic Methylammonium Lead Iodide Between 100 and 352 K. *Chem. Commun.* **2015**, *51*, 4180–4183.

(35) Landsberg, P. T. *Recombination in Semiconductors*; Cambridge University Press: Cambridge, 1991.

(36) Löper, P.; Stuckelberger, M.; Niesen, B.; Werner, J.; Filipič, M.; Moon, S.-J.; Yum, J.-H.; Topič, M.; De Wolf, S.; Ballif, C. Complex Refractive Index Spectra of $CH_3NH_3PbI_3$ Perovskite Thin Films Determined by Spectroscopic Ellipsometry and Spectrophotometry. *J. Phys. Chem. Lett.* **2015**, *6*, 66–71.